Interaction of Water with Sodium Bis(2-ethyl-1-hexyl) Sulfosuccinate in Reversed Micelles

H. Hauser,*,† G. Haering,‡ A. Pande,‡,§ and P. L. Luisi‡

Laboratorium für Biochemie and Institut für Polymere, ETH Zürich, ETH-Zentrum, CH-8092 Zürich, Switzerland *(Received: May 1, 1989)*

The hydration of sodium bis(2-ethyl-1-hexyl) sulfosuccinate (AOT) reversed micelles has been studied by three independent methods: differential scanning calorimetry, ESR spin labeling, and ^2H NMR. A consistent picture is evolving although the actual hydration numbers differ from method to method. This difference is most likely due to differences in the principles underlying these methods. From both calorimetry and ^2H NMR it is concluded that two water molecules are tightly bound to one AOT-Na^+ molecule whereas ESR spin labeling identifies four strongly bound water molecules. Our calorimetric study benefited greatly from a comparison of the thermal behavior of AOT reversed micelles and AOT smectic (lamellar) phases. Calorimetry reveals that six water molecules are unfreezable in AOT reversed micelles. This is also the case for AOT smectic (lamellar) phases; however, these six water molecules can be frozen by cooling the sample to -40 °C. The difference in the two AOT systems is attributed to supercooling that takes place in the submicroscopic droplets of AOT reversed micelles. ^2H NMR gives further insight into AOT hydration. A total number of 13 water molecules are affected and structurally perturbed by 1 AOT molecule. These 13 water molecules consist of three types of water differing in the affinity for AOT-Na^+. Two out of these 13 water molecules are more strongly bound; the remaining 11 water molecules appear to be weakly associated with AOT-Na^+.

Introduction

Surfactants such as sodium bis(2-ethyl-1-hexyl) sulfosuccinate (AOT) aggregate in apolar solvents and have the remarkable property of solubilizing large quantities of water. The resulting clear isotropic solution is referred to as reversed micelles at low water contents $W_0 = [H_2O]/[AOT] < 15$ whereas the term water-in-oil microemulsion is preferred at higher W_0 values. These systems have been studied extensively over the past two decades by use of a great number of physicochemical methods.[1-3] It is now well established that AOT reversed micelles in isooctane consist of an approximately spherical water core surrounded by closed AOT aggregates.[4] An important property of AOT reversed micelles is the amount and the nature of the solubilized water. There is an apparent linear relationship between $W_0 = [H_2O]/[AOT]$ and the radius R_c of the water core,[4-6] and R_c values in excess of 10 nm at $W_0 \geq 40$ were reported.[4] Reversed micelles and water-in-oil microemulsions in general can be used to solubilize biopolymers such as proteins, enzymes,[7-9] and genetic material[10] in "apolar solvents" and to study their physicochemical properties in the presence of limited amounts of water. The guest molecules are either dissolved in the water core or oriented at the AOT-water interface. They may acquire characteristic properties and reactivities[10] different from those measured in the bulk aqueous phase. Reversed micelles and water-in-oil microemulsions have therefore recently become important as models for enzyme catalysis[11] and membrane transport,[12] in the study of light-induced charge separation, and more general in research of energy conversion and transduction.[13]

It is now well established by using a variety of physical techniques that part of the water present in the water core of reversed micelles is bound to the AOT polar group and the sodium counterion. By use of spectroscopic techniques such as NMR,[14-20] ESR spin labeling,[21-23] IR and Raman spectroscopy,[24,25] it has been shown that the physicochemical properties of AOT reversed micelles change markedly at low water contents up to molar ratios $W_0 = 6-10$. Above these W_0 values, the changes with increasing water content become smaller and the properties of the solubilized water approach those of the bulk water. This finding has been interpreted to indicate that water up to $W_0 = 6-10$ is structured due to its interaction with Na^+ counterions and the strong dipole of the AOT polar group. The water up to $W_0 < 10$ is therefore structurally and motionally different from unperturbed bulk water.

The main aim of this work is to determine the amount of perturbed water, i.e., the amount of water bound to the AOT polar group in the ternary system AOT-isooctane-water. Furthermore, the question of whether this water occurs in different hydration shells will be addressed. Three different techniques will be used to shed light on these questions: differential scanning calorimetry (DSC), ESR spin labeling, and ^2H NMR using ^2H_2O as an isotopic replacement of H_2O. ^2H NMR was applied successfully to the question of phospholipid hydration.[26-29] It not only yielded

* To whom correspondence should be addressed.
† Laboratorium für Biochemie.
‡ Institut für Polymere.
§ Present address: Eye Research Institute, 20 Staniford St., Boston, MA 02114.

(1) Eicke, H.-F. *Top. Curr. Chem.* **1980**, *87*, 85.
(2) Luisi, P. L.; Magid, L. J. *CRC Crit. Rev. Biochem.* **1986**, *20*, 409.
(3) Robb, I. D. *Microemulsions*; Plenum Press: New York, 1982.
(4) Zulauf, M.; Eicke, H.-F. *J. Phys. Chem.* **1979**, *83*, 480.
(5) Menger, F. M.; Donohue, J. A.; Williams, R. F. *J. Am. Chem. Soc.* **1973**, *95*, 286.
(6) Robinson, B. H.; Toprakcioglu, C.; Dore, J. C. *J. Chem. Soc., Faraday Trans. 1* **1984**, *80*, 13.
(7) Luisi, P. L. *Angew. Chem.* **1985**, *6*, 449.
(8) Martinek, K.; Levashov, A. V.; Klyachko, N.; Khmelnitski, Y. L.; Berezin, I. V. *Eur. J. Biochem.* **1986**, *155*, 453.
(9) Imre, V. E.; Luisi, P. L. *Biochem. Biophys. Res. Commun.* **1982**, *107*, 538.
(10) Fendler, J. In *Catalysis in Micellar and Macromolecular Systems*; Academic Press: New York, 1975.
(11) Menger, F.; Yamada, K. J. *J. Am. Chem. Soc.* **1979**, *101*, 6731.
(12) Fendler, J. H. *J. Phys. Chem.* **1980**, *84*, 1484.
(13) Monserrat, K.; Grätzel, M.; Tundo, P. *J. Am. Chem. Soc.* **1980**, *102*, 5507.
(14) Frank, S. G.; Zografi, G. *J. Colloid Interface Sci.* **1968**, *28*, 66.
(15) Wong, M.; Thomas, J. K.; Nowak, T. *J. Am. Chem. Soc.* **1977**, *99*, 4730.
(16) Martin, C. A.; Magid, L. J. *J. Phys. Chem.* **1981**, *85*, 3938.
(17) Maitra, A. N. *J. Phys. Chem.* **1984**, *88*, 5122.
(18) Carnali, J.; Lindmann, B.; Södermann, O.; Walderhaug, H. *Langmuir* **1986**, *2*, 51.
(19) Llor, A.; Rigny, P. *J. Am. Chem. Soc.* **1986**, *108*, 7533.
(20) De Marco, A.; Menegatti, E.; Luisi, P. L. *J. Biochem. Biophys. Methods* **1986**, *12*, 325.
(21) Menger, F. M.; Saito, G.; Sanzero, G. V.; Dodd, J. R. *J. Am. Chem. Soc.* **1975**, *97*, 909.
(22) Barelli, A.; Eicke, H.-F. *Langmuir* **1986**, *2*, 780.
(23) Haering, G.; Luisi, P. L.; Hauser, H. *J. Phys. Chem.* **1988**, *92*, 3574.
(24) MacDonald, H.; Bedwell, B.; Gulari, E. *Langmuir* **1986**, *2*, 704.
(25) D'Aprano, A.; Lizzio, A.; Turco Liveri, V.; Aliotta, F.; Vasi, C.; Migliardo, P. *J. Phys. Chem.* **1988**, *92*, 4436.
(26) Veksli, Z.; Salsbury, N. J.; Chapman, D. *Biochim. Biophys. Acta* **1969**, *183*, 434.
(27) Finer, E. G.; Darke, A. *Chem. Phys. Lipids* **1974**, *12*, 1.
(28) Finer, E. G. *J. Chem. Soc., Faraday Trans. 2* **1973**, *69*, 1590.
(29) Hauser, H., In *Water: A Comprehensive Treatise*; Franks, F., Ed.; Plenum Press: New York and London, 1974; Vol. 4, p 209.

0022-3654/89/2093-7869$01.50/0

information concerning the amount of bound water but also provided evidence for several types of bound water differing in motional characteristics.[27-29]

Experimental Section

Materials. Sodium bis(2-ethyl-1-hexyl) sulfosuccinate (AOT) was purchased from Sigma and 4-[(*N*,*N*-dimethyl-*N*-hexadecyl)ammonio]-2,2,6,6-tetramethylpiperidine-1-oxyl iodide (CAT 16; see Figure 1 in ref 23) from Molecular Probes, Eugene, OR; both compounds were used without further purification. Isooctane (puriss. grade) was from Fluka and also used as supplied. Water was deionized and double distilled in an all-glass apparatus and had an apparent pH of 6.3. ^2H_2O (99.9%) and perdeuterated isooctane were purchased from E. Merck, Darmstadt, FRG.

Methods. AOT reversed micelles in isooctane containing the desired amount of H_2O or ^2H_2O were prepared as described before.[30] The appropriate amounts of H_2O or ^2H_2O (for ^2H NMR) were injected into AOT solutions in isooctane by use of a Hamilton syringe.

Differential Scanning Calorimetry (DSC). Differential scanning calorimetry was performed with a Perkin Elmer DSC-2 calorimeter. The reversed micellar dispersion (50 μL) containing 20, 50, or 100 mM AOT was injected into a stainless steel DSC pan that was sealed immediately. In the reference pan the corresponding solution of AOT in isooctane without H_2O was used. Aqueous dispersions of AOT (without isooctane) for calorimetric measurements were prepared by weighing solid AOT into the DSC pan and adding the appropriate amount of H_2O with a Hamilton syringe. The pan was sealed immediately and transferred to the calorimeter. With these dispersions empty reference pans were used. Samples were first cooled to about −30 to −40 °C and subsequently heated. The heating rate was 1–5 °C/min. Since identical results were obtained regardless of the heating rate, 2.5 °C/min was used routinely. The peak in the heat capacity vs temperature plot was integrated to yield the transition enthalpy ΔH using a Perkin-Elmer Model 3600 data station. The weight of H_2O present in the DSC pan was taken from the analytical composition of the AOT reversed micelles or aqueous AOT dispersions.

Electron Spin Resonance (ESR) Spin Labeling. ESR spectra were recorded at 9.2 GHz with a Varian X-band spectrometer (Model E-104A) fitted with variable-temperature equipment. Experimental details have been given previously.[23,31] ESR spectra of CAT 16 incorporated into AOT reversed micelles were treated in terms of fast and to a first approximation isotropic motion with reorientational correlation times of <3 ns using the theory of Kivelson.[32,33]

$$\tau_c = (6.5 \times 10^{10}) W[(h_0/h_{-1})^{1/2} - 1] \quad (1)$$

where W is the peak-to-peak width of the center line ($m_I = 0$) and h_0 and h_{-1} are the peak heights of the center line and high-field line ($m_I = 1$), respectively.

Deuterium Magnetic Resonance Spectroscopy (^2H NMR). ^2H NMR spectra of AOT reversed micelles containing different quantities of ^2H_2O were recorded at 46.072 MHz by use of a Bruker AM 300 WP Fourier transform spectrometer. The amount of ^2H_2O incorporated into AOT reversed micelles ranged from $W_0 = 1$ to $W_0 = 50$. At all W_0 values, ^2H_2O incorporated into AOT reversed micelles gave rise to a singlet, no quadrupole splitting being observed. The chemical shift of the singlet was referenced relative to the most intensive ^2H NMR signal of the naturally occurring ^2H isotope of isooctane. At low water contents ($W_0 \leq 3$), about 1000 free induction decays were used (acquisition time ≈ 0.5 s). Since the ^2H NMR spectra were recorded without field-frequency lock, the accuracy of the chemical shift measurements and particularly of the line-width measurements was limited.

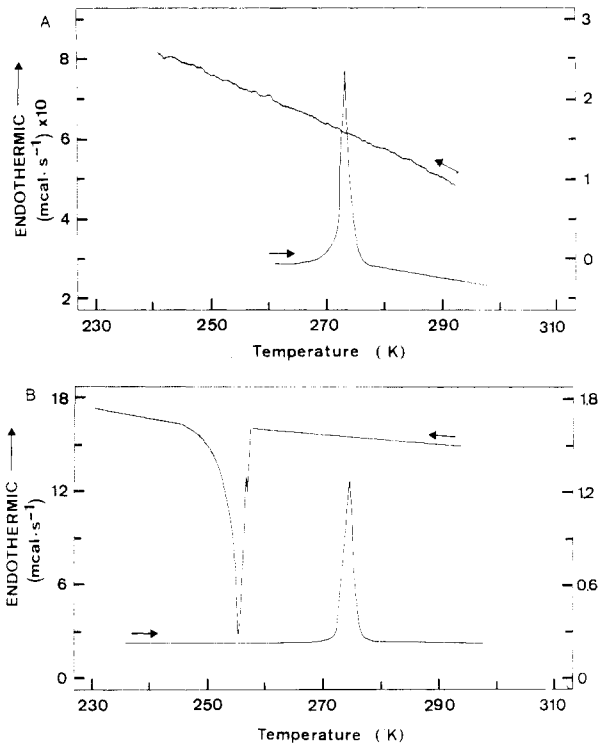

Figure 1. DSC curves of AOT reversed micelles. (A) Heating and cooling curves of AOT reversed micelles in isooctane, [AOT] = 0.15 M, $W_0 = [H_2O]/[AOT] = 10$, recorded at 2.5 °C/min. (B) Heating and cooling curves of AOT reversed micelles in isooctane; the experimental conditions were as in (A) except that $W_0 = 50$. The ordinate on the left refers to heating and the ordinate on the right to cooling.

Results

Differential Scanning Calorimetry (DSC). Reversed micelles (or microemulsions) consisting of 50 mM AOT in isooctane and increasing amounts of H_2O ($1 \leq W_0 \leq 50$) were examined by DSC. Samples were inserted into the DSC instrument at room temperature and first cooled to about −30 to −40 °C. As shown in Figure 1A, reversed micelles with $W_0 < 10$ showed no apparent exothermic event upon cooling the sample to −30 °C. In contrast AOT reversed micelles containing water in excess of $W_0 \sim 10$ exhibited an exothermic transition when cooled from room temperature (Figure 1B). The subsequent heating run gave an endothermic transition at 0 °C that can be assigned to the melting of ice (Figure 1A). Large hysteresis effects were observed. For example, at $W_0 = 50$ the exothermic peak assigned to ice formation occurred at −18 °C (Figure 1B). The temperature of ice formation decreased even further with decreasing water content W_0, and the enthalpy ΔH associated with this event showed the same trend (data not shown). The marked supercooling is a phenomenon well documented in the literature[34,35] and may be attributed to the small volume of free water. The ice-melting peak at 0 °C was recorded upon subsequent heating, and the enthalpy ΔH of the ice-melting peak was plotted as a function of W_0 (data not shown). A least-squares fit to the experimental data points yielded a straight-line relationship with $r^2 = 0.99$. Extrapolation of this straight line to $\Delta H \rightarrow 0$ gave as the intercept on the W_0 axis a value of $W_0 = 6.1 \pm 0.2$. This value may be identified as the amount of unfreezable water. From the slope of the straight-line relationship the enthalpy ΔH of the ice-melting peak can be obtained. The value of 76 ± 3 cal/g derived in this way is in reasonably good agreement with the theoretical value of 79.7 cal/g.[36]

(30) Wolf, R.; Luisi, P. L. *Biochem. Biophys. Res. Commun.* **1979**, *89*, 209.
(31) Hauser, H.; Gains, N.; Semenza, G.; Spiess, M. *Biochemistry* **1982**, *21*, 5621.
(32) Kivelson, D. *J. Chem. Phys.* **1960**, *33*, 1094.
(33) Stone, T. J.; Buckman, T.; Nordio, P. L.; McConnell, H. M. *Proc. Natl. Acad. Sci. U.S.A.* **1965**, *54*, 1010.
(34) Broto, F.; Clausse, D. *J. Phys.* **1976**, *9*, 4251.
(35) Boned, C.; Peyrelasse, J.; Moha-Ouchasse, M. *J. Phys. Chem.* **1986**, *90*, 634.

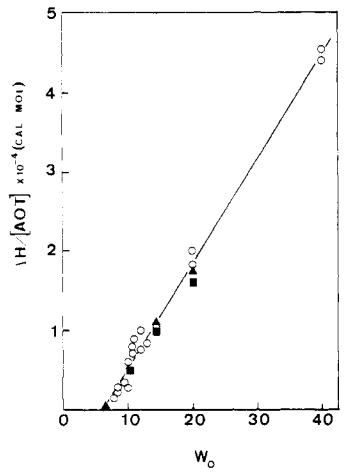

Figure 2. Normalized enthalpies $\Delta H/[AOT]$ as a function of the water content $W_0 = [H_2O]/[AOT]$ of AOT reversed micelles in isooctane. The enthalpy of ΔH of the melting of ice at 0 °C was determined by differential scanning calorimetry (DSC) after cooling the AOT reversed micelles to about −30 to −40 °C. Reversed micelles of different AOT concentrations were used: 20 mM AOT (■), 50 mM AOT (▲), and 100 mM AOT (○). The water content of the AOT reversed micelles varied between $W_0 = 6$ and $W_0 = 40$.

The DSC experiments described above were extended to AOT reversed micelles differing in AOT concentrations. At each concentration a straight-line relationship was obtained when the transition enthalpy ΔH was plotted as a function of W_0. In order to present all data on one graph, the transition enthalpies ΔH were normalized with respect to the AOT concentration as shown in Figure 2. The data were best fitted by a linear regression analysis yielding the solid line in Figure 2. Extrapolation of this line to $\Delta H/[AOT] \rightarrow 0$ yielded as the intercept $W_0 = 6.0 \pm 0.1$.

The thermal behavior of AOT reversed micelles was compared with that of AOT dispersions. The latter were made as described under Methods, the main difference being that AOT is dispersed directly in H_2O, i.e., in the absence of isooctane. Aqueous AOT dispersions form a smectic (lamellar) phase under the experimental condition used here.[37,38] The main feature of the thermogram of aqueous AOT dispersions is illustrated in Figure 3: three transitions are observed upon heating. In excess water (Figure 3A) there are two minor events below 0 °C and a main transition between 0 and 3 °C. This result agrees qualitatively with the results reported by Czarniecki et al.[37] The main transition at 0–3 °C can be assigned to the melting of ordinary ice. In Figure 4 the enthalpy values of this ice-melting peak are plotted as a function of the AOT concentration. It is possible to include in this plot the ΔH values of the melting of ice in AOT reversed micelles. To do so the AOT in reversed micelles is referred to the sum of the weight of AOT and water; i.e., AOT reversed micelles are treated as a two-phase system consisting of an aqueous phase and an isooctane phase separated by a monolayer of AOT. The graph in Figure 4 is nonlinear and differs in this respect from the plot reported by Czarniecki et al.[37] The reason for this discrepancy is unknown. The solid curve (Figure 4) representing the best fit to the experimental data extrapolates to about 80% AOT at $\Delta H \rightarrow 0$ corresponding to 6.2 water molecules per molecule AOT. This result is interpreted to mean that, as in AOT reversed micelles, in aqueous AOT dispersions all water except about six water molecules per AOT molecule freeze and form ordinary ice upon cooling. Apparently, the "unfreezable" water is sufficiently strongly bound to AOT and/or the Na^+ counterion so that the formation of ordinary ice is prevented. The two minor transitions below 0 °C occur at −7 ± 1 °C and −11 ± 0.5 °C (cf.

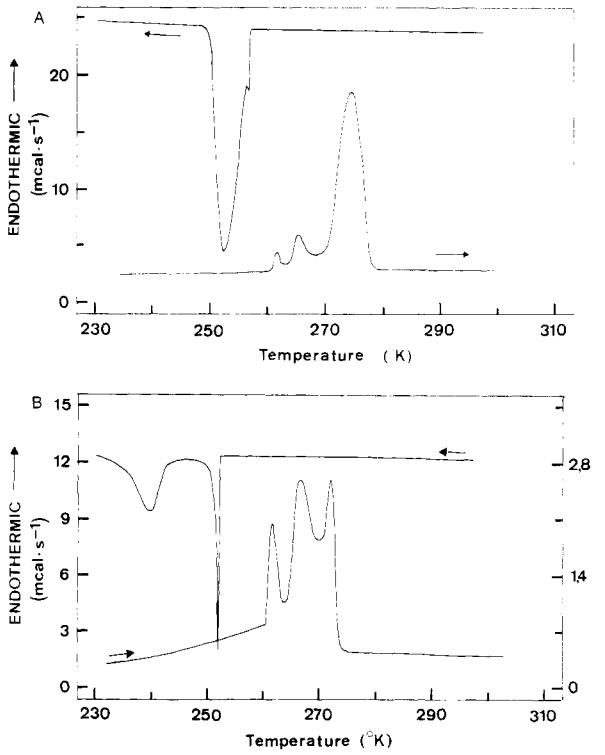

Figure 3. DSC curves of aqueous AOT dispersions in the absence of isooctane. (A) Heating and cooling curves of a 40% AOT dispersion in H_2O. (B) Heating and cooling curves of a 70% AOT dispersion in H_2O. Both samples were scanned at 2.5 °C/min. The ordinate on the left refers to cooling and that on the right to heating.

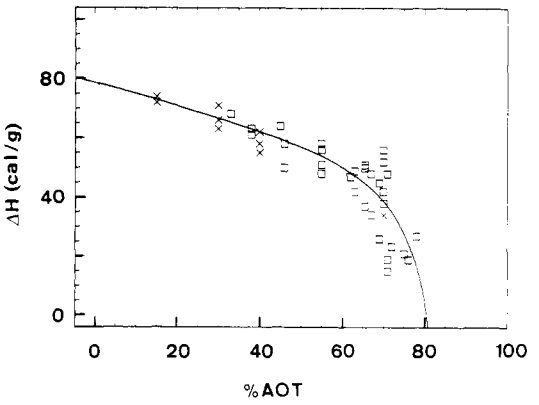

Figure 4. Enthalpy ΔH (cal/g) of the ice-melting peak at 0 °C of aqueous AOT dispersions (×) and AOT reversed micelles in isooctane (□) as a function of the AOT concentration expressed as percent. In case of AOT reversed micelles AOT is referred to the sum of the weight of AOT and water.

Figure 3). The sum of their enthalpies increases with increasing AOT concentration at the expense of the enthalpy of the ice-melting peak at about 0 °C. This is evident from a comparison of Figure 3A and Figure 3B. Integration of these two subzero transitions (Figure 3) yields a value for the total enthalpy of 8.8 ± 0.2 kcal/mol AOT corresponding to about six water molecules per AOT molecule. On the basis of this result and two observations discussed below the two subzero transitions are tentatively assigned to bound water that "melts" at temperatures significantly below the melting of ordinary ice. The following observations support this assignment:

(1) An AOT dispersion in ^2H_2O gave the same thermogram as that shown in Figure 3A except that all three peaks were shifted to higher temperatures by about 4 °C. This is expected if the transitions were all due to water.

(2) When a 70% dispersion of AOT in glycerol was cooled to −40 °C, upon heating no endothermic transition occurred between −40 and 100 °C. This observation also suggests that the two minor

(36) *Handbook of Chemistry and Physics*, 55th ed.; Weast, R. C., Ed.; CRC Press: Cleveland, OH, 1974–1975; p B244.

(37) Czarniecki, K.; Jaich, A.; Janik, J. M.; Rachwalska, M.; Janik, J. A.; Krawczyk, J.; Otnes, K.; Volino, F.; Ramasseul, R. *J. Colloid Interface Sci.* **1983**, *92*, 358.

(38) Rogers, J.; Winsor, P. A. *Nature (London)* **1967**, *216*, 477.

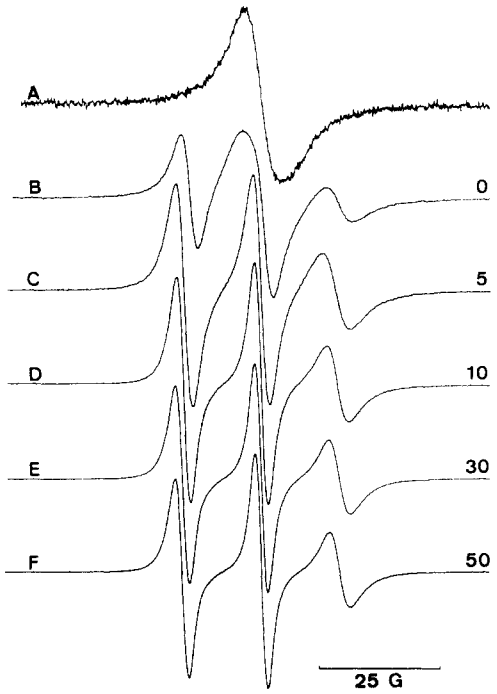

Figure 5. ESR spectra of CAT 16. (A) CAT 16 dispersed in pure isooctane; (B) CAT 16 in AOT reversed micelles in isooctane containing 0.15 M AOT, [AOT]/[spin label] = 300, W_0 = 0; (C), (D), (E), and (F) same as B except that W_0 = 5, 10, 30, and 50, respectively. The water content expressed as W_0 is given on the right-hand side of each spectrum.

endotherms in Figure 3A are due to water and not to AOT.

ESR Spin Labeling. The spin label 4-[(*N*,*N*-dimethyl-*N*-hexadecyl)ammonio]-2,2,6,6-tetramethylpiperidine-1-oxyl iodide (CAT 16) is insoluble in isooctane as is evident from the ESR spectrum of a CAT 16 dispersion in this solvent (Figure 5, top spectrum). It consists of a broad single resonance line characteristic of Heissenberg spin exchange indicating that the spin label does not dissolve in isooctane but is present as aggregates, probably as microcrystals. This is contrasted by a three-line ESR spectrum when CAT 16 was added to AOT reversed micelles in isooctane in the absence of water (Figure 5, W_0 = 0). The three-line spectrum is apparently superimposed on a spin-exchange component. With increasing water content (W_0 = 5–50) the latter disappeared and the line width of the three-line spectrum decreased, indicating that the tumbling motion of the spin probe increased with increasing W_0. In analogy to other amphiphilic, surface-active spin labels, and based furthermore on previous results[23] as well as on spectral parameters such as the hyperfine coupling constants, it is reasonable to assume that CAT 16 is incorporated in the AOT monolayer with its polar group being anchored at the AOT–water interface. Under these conditions, contributions to the ESR spectrum from exchange of CAT 16 between different compartments of the AOT reversed micelles can be ruled out and the ESR spectra may be evaluated in terms of effective rotational correlation times τ_c according to the theory of Kivelson.[32,33]

Effective correlation times τ_c derived from the ESR spectra as described under Methods are shown as a function of W_0 in Figure 6. At low water content (up to $W_0 \approx 5$), τ_c is about equal to the correlation time of tumbling of the overall micelle. An estimate for τ_c of micelle tumbling is obtained from the Stokes–Einstein equation

$$\tau_c = 4\pi R_h^3 \eta / 3kT \qquad (2)$$

where R_h is the hydrodynamic radius of the reversed micelle which is the sum of the hydrodynamic radius R_c of the water core and the thickness d of the AOT monolayer (in angstroms): $R_h = R_c + d = 1.5W_0 + d$;[39] η is the viscosity and k and T have their usual meaning. Inserting the following values into eq 2, W_0 = 4, R_h = 17 Å (d = 11 Å) and η = 0.38 cP, yields $\tau_c \approx 2$ ns. A comparison of this value with the experiment (Figure 6) indicates that the spin-label motion at low W_0 values is dominated by the overall tumbling of the AOT reversed micelle. Figure 6 shows that the correlation time τ_c decreases markedly up to $W_0 \approx 10$. At higher water contents ($W_0 \geq 10$) the curve in Figure 6 flattens out, indicating that τ_c changes little with increasing water contents.

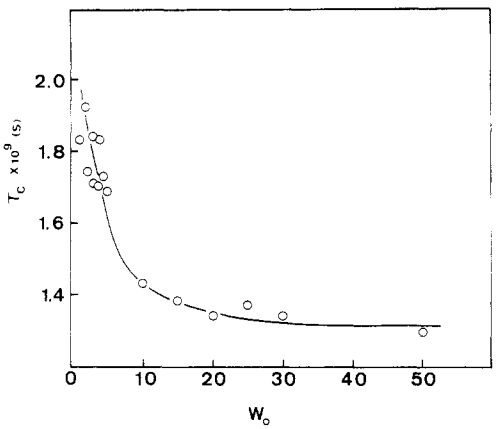

Figure 6. Rotational correlation times τ_c as a function of water content expressed as W_0. AOT reversed micelles ([AOT] = 0.15 M) differing in water content W_0 were labeled with CAT 16 so that the molar ratio [AOT]/[spin label] = 300. From the ESR spectra (cf. Figure 5) rotational correlation time τ_c were derived by use of eq 1.

The graph in Figure 6 may be modeled assuming that the spin probe experiences two different environments. The observed correlation time τ_c is then given by

$$\tau_c = \tau_b f_b + \tau_f f_f \qquad (3)$$

where τ_b and τ_f are the correlation times for motion of the inverted micelle as a whole (on the order of 2 ns) and the spin probe present in the fully hydrated micelle, respectively, and f_b and f_f are the fractions of bound and free water, respectively. Introducing the hydration number $r = [H_2O]_b/[AOT]_t$, where $[H_2O]_b$ and $[AOT]_t$ are the concentrations of bound water and total AOT, respectively, eq 3 can be rearranged:

$$\tau_c = (\tau_b - \tau_f)\frac{r}{W_0} + \tau_f \qquad (4)$$

The solid line in Figure 6 represents the best fit to the experimental data points yielding values for r = 3.8, τ_b = 1.8 ns, and τ_f = 1.26 ns.

Deuterium Magnetic Resonance Spectroscopy (^2H NMR). ^2H_2O incorporated into AOT reversed micelles gave rise to a single deuterium signal over the total ^2H_2O concentration range studied (W_0 varied between 1 and 50): no quadrupole splitting was observed. Representative ^2H NMR spectra are shown in Figure 7. A Langmuir-type curve was obtained by plotting the chemical shift δ of the ^2H_2O signal as a function of W_0 (Figure 8A). At $W_0 > 50$, the chemical shift δ approached a value which is similar to that of pure ^2H_2O (183 Hz, relative to the most intensive signal of perdeuterated isooctane as an internal chemical shift standard). The line width $\Delta\nu_{1/2}$ decreased sharply with increasing water content up to $W_0 \approx 6$; above this water content there was little further change in $\Delta\nu_{1/2}$, which approached a limiting value of about 2 Hz. This is close to the value measured in pure ^2H_2O (Figure 8B; cf. Figure 7).

In the following analysis of the chemical shift data it is assumed that ^2H_2O is bound to the AOT polar group in p different hydration shells, each containing n_i water molecules with a characteristic chemical shift δ_i. Provided that the binding sites are independent and that there is fast exchange between binding sites, then the observed chemical shift δ is the weighted average of the characteristic chemical shift δ_i. That there is indeed fast exchange between bound water and bulk water in AOT reversed micelles is evident from the fact that only a single ^2H NMR signal is

(39) Yoshioka, H. *J. Colloid Interface Sci.* **1983**, *95*, 81.

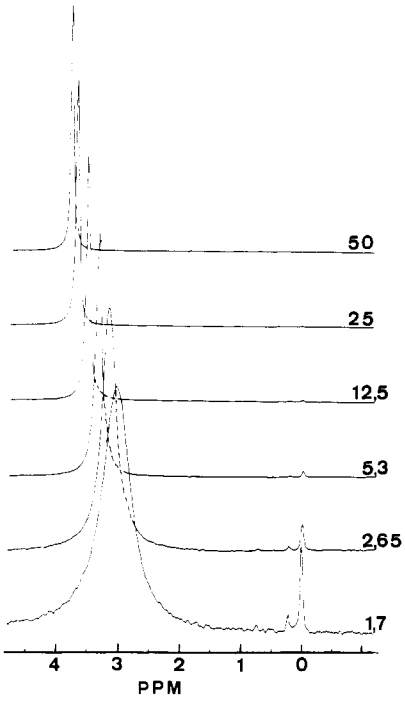

Figure 7. Deuterium magnetic resonance (^2H NMR) spectra of AOT reversed micelles in isooctane containing increasing quantities of ^2H_2O. The amount of ^2H_2O solubilized in the reversed micelles is expressed as W_0 given on the right-hand side of each spectrum. NMR spectra were recorded at 46.072 MHz and 24 °C with a Bruker AM 300 WP Fourier transform spectrometer. The chemical shift of the single ^2H_2O signal was measured relative to the most intensive ^2H signal of isooctane present in natural abundance.

observed at all ^2H_2O contents (Figure 7).

The chemical shift data can be analyzed by use of the mass equation. For each of the p hydration shells with n_i identical independent binding sites for H_2O per AOT molecule, the mass equation is applied:

$$\mathrm{AOT} + \mathrm{H_2O} \rightleftharpoons \mathrm{AOT\text{-}H_2O};\quad K_1 = \frac{[\mathrm{AOT\text{-}H_2O}]}{[\mathrm{AOT}][\mathrm{H_2O}]} \tag{5}$$

$$\mathrm{AOT\text{-}H_2O} + \mathrm{H_2O} \rightleftharpoons \mathrm{AOT\text{-}(H_2O)_2};\quad K_2 = \frac{[\mathrm{AOT\text{-}(H_2O)_2}]}{[\mathrm{AOT\text{-}H_2O}][\mathrm{H_2O}]} \tag{6}$$

$$\mathrm{AOT\text{-}(H_2O)_{n-1}} + \mathrm{H_2O} \rightleftharpoons \mathrm{AOT\text{-}(H_2O)_n};\quad K_n = \frac{[\mathrm{AOT\text{-}(H_2O)_{n-1}}]}{[\mathrm{AOT\text{-}(H_2O)_n}][\mathrm{H_2O}]} \tag{7}$$

where K_1, K_2, ..., K_n are the equilibrium constants for the consecutive reactions, [AOT] and [H_2O] are the AOT and H_2O concentrations (activities), respectively, and [AOT-H_2O], [AOT-$(H_2O)_2$], [AOT-$(H_2O)_n$] are the concentrations (activities) of the different AOT-H_2O complexes. For n identical, independent binding sites of each of the p hydration shells there is a statistical relationship between the different equilibrium constants K_1, K_2, ..., K_n and the intrinsic binding constant K_A[40,41]

$$K_i = [(n - i + 1)i^{-1}]K_A \qquad (i = 1, 2, ..., n) \tag{8}$$

Using this relation together with the mass-action law yields eq 9, known as the Scatchard plot:[40,42]

$$r = \frac{nK_A[\mathrm{H_2O}]_f}{1 + K_A[\mathrm{H_2O}]_f} \quad \text{or} \quad \frac{r}{[\mathrm{H_2O}]_f} = nK_A - rK_A \tag{9}$$

where $r = [H_2O]_b/[AOT]_t$ as defined above, $[H_2O]_f$ and $[H_2O]_b$ are the concentrations of the free and bound water, respectively, and $[AOT]_t$ is the total AOT concentration.

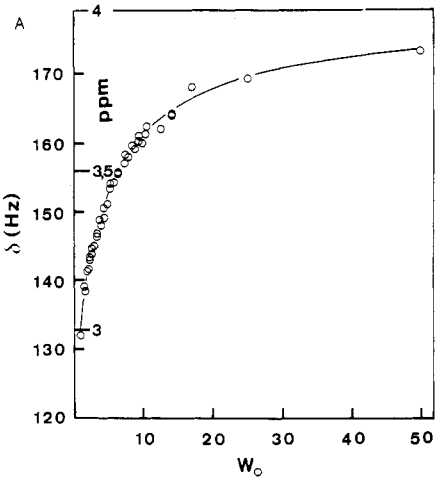

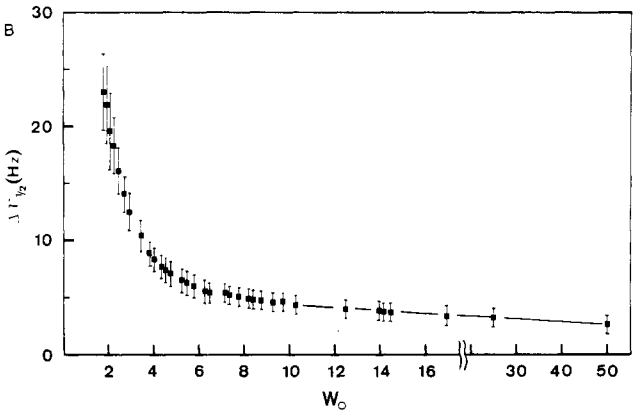

Figure 8. Chemical shifts δ (Hz or ppm) (A) and line width $\Delta\nu_{1/2}$ (Hz) (B) of the ^2H_2O signal of AOT reversed micelles in isooctane as a function of the ^2H_2O content expressed as W_0. The data were derived from the ^2H NMR spectra of AOT reversed micelles in isooctane shown in Figure 7. The chemical shift of the single ^2H_2O signal was measured relative to the main ^2H NMR signal of isooctane present in natural abundance, and the width of this signal was measured at half-height.

Equation 9 holds for one class of n independent binding sites. Next we consider p hydration shells, each with n_i binding sites for water with an intrinsic binding (association) constant K_{Ai}. In this case an equation analogous to eq 9 holds for each class of independent binding sites, and r and $r/[H_2O]_f$ are conveniently expressed parametrically as[43,44]

$$r = \sum_1^p \frac{n_i K_{Ai}[\mathrm{H_2O}]_f}{1 + K_{Ai}[\mathrm{H_2O}]_f} \tag{10}$$

$$\frac{r}{[\mathrm{H_2O}]_f} = \sum_1^p \frac{n_i K_{Ai}}{1 + K_{Ai}[\mathrm{H_2O}]_f} \tag{11}$$

where the subscript i refers to a particular class of intrinsic binding constants K_{Ai}. The fraction f_b of bound water is

$$f_b = \frac{[\mathrm{H_2O}]_b}{[\mathrm{H_2O}]_t} = \frac{\delta_{obs} - \delta_f}{\delta_b - \delta_f} \tag{12}$$

where δ_{obs}, δ_f, and δ_b are the observed chemical shift, the chemical shift of the free ^2H_2O, and the chemical shift of the bound ^2H_2O, respectively; δ_f = 183 Hz, which is identical with the chemical shift of free ^2H_2O relative to deuterated isooctane. A value for δ_b is derived from the Langmuir plot shown in Figure 8A assuming that at low water content (W_0 = 1) all the water is bound, δ_b =

(40) Edsall, J. T.; Wyman, Y. In *Biophysical Chemistry*; Academic Press: New York, 1958; Vol. 1, Chapter 11, p 591.
(41) Hauser, H.; Chapmann, D.; Dawson, R. M. C. *Biochim. Biophys. Acta* **1969**, *183*, 320.
(42) Scatchard, G. *Ann. N.Y. Acad. Sci.* **1949**, *51*, 660.
(43) Cantor, C. R.; Schimmel, P. R. In *Biophysical Chemistry*; W. H. Freeman: San Francisco, 1980; Part III, p 852.
(44) Schreier, A. A.; Schimmel, P. R. *J. Mol. Biol.* **1974**, *86*, 601.

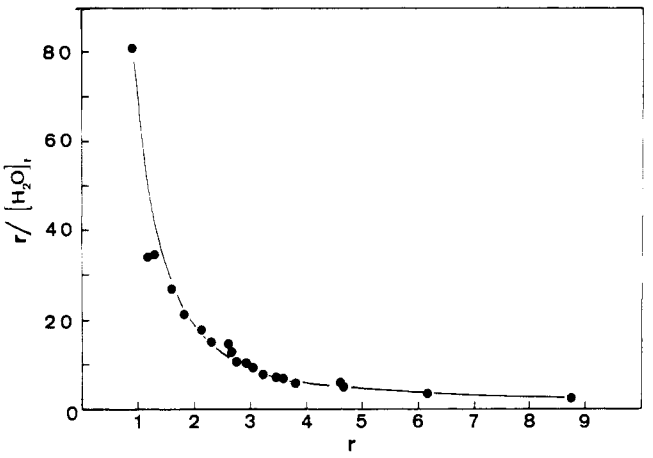

Figure 9. Scatchard plot constructed from the ^2H chemical shift data shown in Figure 8A. $r/[H_2O]_f$ is plotted as a function of r and evaluated according to eq 10 and 11. The solid line represents the computer fit to the experimental data, and the n_i and K_{Ai} values derived from this fit are summarized in Table I.

TABLE I: Hydration Numbers and Hydration Shells of AOT

r^a	n_i^b	K_{Ai}, M^{-1}	method
6	$n_1 = 2$		DSC
	$n_2 = 4$		
4			ESR spin labeling
13	$n_1 = 1$	$K_{A1} = 200$	^2H NMR
	$n_2 = 1$	$K_{A2} = 15$	
	$n_3 = 11$	$K_{A3} = 0.36$	

$^a r = [H_2O]_b/[AOT]_t$. $^b n_i$ are he hydration shells, i.e., different classes of binding sites of AOT for H_2O that are characterized by the intrinsic binding constant K_{Ai}. The n_i and K_{Ai} values were derived from the computer simulation of the curved Scatchard plot (Figure 9) using eq 10 and 11.

125 Hz (Figure 8A). With these values for δ_f and δ_b and knowing $[H_2O]_t$ and $[AOT]_t$ from the analytical composition of the reversed micelles, for each value of δ_{obs} the concentration of bound water $[H_2O]_b$ is calculated by using eq 12. Calculating $r = [H_2O]_b/[AOT]_t$ and $[H_2O]_f = [H_2O]_t - [H_2O]_b$ and plotting the data as a Scatchard plot according to eq 9 should yield a straight line in the case of n identical, independent binding sites. The Scatchard plot thus derived from the chemical shift data is, however, not linear but curved, concave upward (Figure 9). This is interpreted to indicate that there are more than one class of binding sites for H_2O. The curved Scatchard plot shown in Figure 9 was decomposed according to methods described in the literature.[42,43,45] As seen in Figure 9, a reasonably good computational fit represented by the solid line (Figure 9) is produced with three classes of different binding sites characterized by the following n_i and K_{Ai} values (Table I): $n_1 = 1$, $K_{A1} = 200$ M^{-1}, $n_2 = 1$, $K_{A2} = 15$ M^{-1}, $n_3 = 11$, $K_{A3} = 0.36$ M^{-1}.

In principle the same method as used above for the evaluation of the chemical shift data should be applicable to the evaluation of the line-width data. Unfortunately these data turned out to be insufficiently accurate to warrant a quantitative interpretation. The lack of accuracy is probably due to the fact that ^2H NMR spectra were recorded without field-frequency lock.

Discussion

A consistent picture is emerging from the application of DSC, ESR spin labeling, and ^2H NMR to the question of hydration of AOT and the state of H_2O in the ternary system AOT–isooctane–water. Our results derived from these three independent methods will be discussed and compared with each other and with data reported in the literature. Our ESR and ^2H NMR measurements are qualitatively in agreement with data in the literature. When physicochemical properties of AOT reversed micelles are investigated as a function of the water content W_0, their water dependence exhibits the characteristic behavior as shown, for instance, for some ESR and NMR parameters in Figures 6 and 8, respectively. The physical properties change significantly up to $W_0 \approx 10$ and level off at higher water contents. The main feature of the graphs depicted in Figures 6 and 8A,B may therefore be regarded as representative. For example, this kind of behavior was reported in fluorescence polarization studies of AOT reversed micelles.[46,47] The mean anisotropy of 3,4,9,10-perylene sodium tetracarboxylate and 9,10-anthracenediacetic acid in AOT reversed micelles decreased markedly up to $W_0 \approx 10$, and approached a plateau at higher water contents. This behavior was also found for the internal relaxation time of these fluorescence probes. Another fluorescence study on AOT reversed micelles in alkane solutions using 1-anilino-8-naphthalenesulfonate (ANS) as a fluorescent label[48] showed that the fluorescence intensity change were most significant up to $W_0 \approx 8$. The authors concluded that water is firmly bound up to $W_0 = 6$ and free water appears when water is present in excess of $W_0 = 12$. A study using solvated electrons as a probe for water dynamics of AOT reversed micelles found that the line width of the absorption spectrum of the hydrated electron decreases with increasing W_0 reaching a plateau at $W_0 = 12$.[49] A study of AOT reversed micelles using time-resolved microwave conductivity measurements showed that the microwave conductivity increases on addition of H_2O up to $W_0 \approx 9$, and then no further changes were observed up to $W_0 = 40$.[50] A proton-transfer study using various fluorescent probes showed that deprotonation rates reach values comparable to those observed in bulk H_2O at $W_0 = 10$–12.[51,52] As expected, similar relationships to those shown in Figure 8 were obtained when ^1H chemical shifts and line widths of the water signal of AOT reversed micelles in isooctane are plotted as a function of W_0.[20] This kind of behavior was also reported in a ^1H and ^{23}Na NMR study of AOT reversed micelles;[15] in this case rotational correlation times τ_c for water protons derived from T_1 measurements and ^{23}Na line widths of the ^{23}Na NMR signals were plotted as a function of W_0. The authors concluded that on completion of the solvation shell of AOT and its Na^+ counterion at about six H_2O molecules per AOT, the rigidity of the micellar core is greatly reduced (cf. also ref 19).

The hydration numbers derived from the three different methods applied here vary between 4 and 13 water molecules bound per AOT molecule. This variation from method to method is not too surprising considering the difference in the basic principles involved, in the sensitivity, and in the assumptions made in the evaluation of the primary data.

DSC is supposed to be a convenient method for determining the amount of unfreezable water, i.e., water that is strongly bound to the polar group of lipid or detergents so that its structural perturbation prevents its crystallization. DSC applied to AOT reversed micelles indicates that about six water molecules per AOT molecule do not freeze even at −40 °C. In samples with water contents in excess of six water molecules per AOT molecule, ice formation occurs (Figure 2) and the properties of water approach those of bulk water. Our DSC results may be compared with two recent DSC studies. In the first one[35] heats of crystallization of H_2O were measured as a function of the water content W_0: it was found that in the ternary system AOT–dodecane–water all the water except for the last 6.5 water molecules and in AOT–isooctane–water all water except for the last 4.5 water molecules freeze upon cooling AOT reversed micelles to −50 °C. It was concluded that these water molecules are so strongly bound to the polar group of AOT–Na^+ that its crystallization is prevented.

(45) Scatchard, G.; Colemann, J. S.; Shen, A. L. *J. Am. Chem. Soc.* **1957**, *79*, 12.
(46) Valeur, B.; Keh, E. *J. Phys. Chem.* **1979**, *83*, 3305.
(47) Keh, E.; Valeur, B. *J. Colloid Interface Sci.* **1981**, *79*, 465.
(48) Wong, M.; Thomas, J. K.; Grätzel, M. *J. Am. Chem. Soc.* **1976**, *98*, 2391.
(49) Pileni, M. P.; Hickel, B.; Ferradini, C.; Pucheault, J. *Chem. Phys. Lett.* **1982**, *92*, 308.
(50) Bakale, G.; Warman, J. M. *J. Phys. Chem.* **1984**, *88*, 2927.
(51) Bardez, E.; Goguillon, B.-T.; Keh, E.; Valeur, B. *J. Phys. Chem.* **1984**, *88*, 1909.
(52) Bardez, E.; Monnier, E.; Valeur, B. *J. Phys. Chem.* **1985**, *89*, 5031.

In the second DSC study[53] the freezing behavior of water was examined in the ternary system AOT–isooctane–^2H_2O. The reversed micelles were cooled down to −75 °C, and it was found that all water in excess of $W_0 = 4.5$ freezes at −41 °C. The reason for the difference in the values for unfreezable water between these studies and ours is unclear presently. One possible explanation could be differences in the experimental protocol. We found, for instance, that the actual value for the heat of crystallization of H_2O is highly sensitive to the scanning rate. Several previous reports on AOT–Na^+ hydration arrived at a hydration number $r = 6$ and tentatively assigned these water molecules to the hydration of the Na^+ counterion.[15,17,19,22,54] This assignment is, however, questionable in light of our data and the fact that Na^+ is largely associated (~70%) with AOT.[37]

All three physical methods used here point to two to four water molecules being tightly bound to AOT-Na^+. These values are consistent with hydration numbers derived from osmotic data.[55] For polystyrenesulfonate resins with Na^+ as the counterion, a hydration number of $r = 2.5$ was obtained. Thermodynamic considerations per se cannot give hydration numbers for individual cations and anions. Separate values for the Na^+ cation and the sulfonate anion can be derived on the basis of reasonable assumptions discussed in ref 55. The resulting hydration numbers are 2.0 water molecules per Na^+ and 0.9 water molecules per $R–SO_3^-$ in good agreement with our result.[55]

The DSC experiments with ternary systems such as AOT–isooctane–water carried out in the way described here may be subject to criticism: before each heating run the reversed micellar dispersion is cooled to at least −30 to −40 °C, which is known to destroy the isotropic micellar phase and induce phase separation. Nevertheless, the data derived from these phase-separated samples are in good agreement with the DSC results obtained with aqueous AOT dispersions in the absence of organic solvent (cf. Figure 4). As shown in Figure 4, AOT reversed micelles and aqueous AOT dispersions (without organic solvent) give a consistent set of data that extrapolate to about 20% bound H_2O or six water molecules bound per AOT molecule. The consistency of the results obtained with the two kinds of dispersions (Figure 4) indicates that our DSC measurements carried out with AOT reversed micelles yield results pertinent to the question of AOT hydration.

In comparing the DSC results obtained with AOT reversed micelles and AOT smectic phases, the absence of the subzero transitions in the thermogram of AOT reversed micelles is striking. It is unclear at present why these transitions do not show up in the heating runs of AOT reversed micelles. One possible explanation is supercooling. It is conceivable that due to the small volume of the aqueous compartments present in AOT reversed micelles the bound water is supercooled to the extent that its freezing occurs below −40 °C. In order to shed light on this question we cooled AOT reversed micelles to −100 °C. Upon subsequent heating a glass transition was observed in some but not all samples; however, transitions similar to the two subzero transitions observed with aqueous AOT dispersions (Figure 3) were absent. In reversed micelles ice formation is supposed to take place via a homogeneous nucleation process whereby spontaneous fluctuations in the liquid initiate the crystallization.[56] The homogeneous nucleation temperature is known to decrease with decreasing droplet size; at atmospheric pressure it is close to −40 °C for droplet sizes on the order of micrometers. When the droplet size becomes smaller than the critical fluctuation wavelength, homogeneous nucleation will not take place and supercooling will continue until, at much lower temperature, a glass transition may occur.[52,56] In contrast to AOT reversed micelles, aqueous AOT dispersions (in the absence of isooctane) are known to form a smectic (lamellar) phase. In such a phase, water is intercalated between swollen AOT lamellae extending largely in two dimensions. With a finite thickness of the intercalated water layer the aqueous space becomes large compared to the submicroscopic water droplets present in AOT reversed micelles. Probably the macroscopic dimensions of the water space in aqueous AOT dispersions are a prerequisite for the two subzero transitions to occur; the difference in the dimensions of the aqueous space may well account for the difference in the DSC behavior of the AOT reversed micelles and aqueous dispersions.

Qualitatively the ESR results agree well with the ^2H NMR data. Up to $W_0 = 10–15$, τ_c values decrease markedly, further additions of water having little effect on the correlation time of motion of CAT 16 (cf. Figure 6). Our ESR results are qualitatively also in good agreement with a recent spin-label study.[22] Probing AOT reversed micelles in isooctane with amphiphilic spin labels, these authors observed discontinuities in W_0-dependent ESR parameters such as the hyperfine splitting constant. The discontinuity at $W_0 = 12$ was interpreted to indicate the first appearance of free water. These authors also showed that the activation energy of the rotational correlation times τ_c for spin labels passes through a maximum at $W_0 = 6$ and decreases sharply between $W_0 = 6$ and $W_0 = 20$.[22] The quantitative evaluation of our ESR results leads to conclusions somewhat different from those derived from the ^2H NMR data (see discussion below). The difference is probably due to the simplifying assumption that the spin label occurs in only two different environments.

The evaluation of the ^2H NMR results shows that there are 13 water molecules bound to AOT and/or its counterion Na^+, two of which appear to be more tightly bound than the remaining 11 water molecules (cf. Table I). Comparing the DSC results with the ^2H NMR data, it is clear that only about half of the water of hydration turns out to be unfreezable upon cooling to about −40 °C. This finding is different from the results obtained with phospholipids: the study of the hydration properties of phosphatidylcholine, one of the major naturally occurring phospholipids, revealed that the amount of bound water determined by ^2H NMR (about 12 water molecules per molecule of phosphatidylcholine) is identical with the amount of unfreezable water.[29,57]

If the above interpretation of the two subzero transitions (observed with the lamellar AOT phase) is correct, information pertinent to the last six unfrozen water molecules of hydration can be derived. Integration of these two subzero peaks reveals that the sum of the peak areas corresponds to six water molecules; the ratio of the peak areas is 1:2, the low-temperature transition at −11 °C therefore corresponding to two and the other transition at −7 °C to four water molecules. According to this tentative assignment the last six water molecules of hydration occur in two different hydration shells which differ in both binding affinity and capacity. The assignment is also consistent with ^2H NMR results showing that two water molecules are more tightly bound to AOT–Na^+. Our hydration number of 13 H_2O/AOT is in good agreement with ^2H and ^{17}O spin–lattice relaxation time measurements on the ternary system AOT–isooctane–^2H_2O.[58] This study arrived at the conclusion that the perturbation of the water structure is short-ranged involving the immediate hydration region of about 15 water molecules per AOT–Na^+. The reorientation time of water of hydration was found to be less than 1 order of magnitude (about a factor of 3) slower than that of bulk ^2H_2O.

In conclusion, although there are a number of scattered reports in the literature dealing with the hydration of AOT–Na^+ in reversed micelles, this subject has not been studied systematically. The application of three independent experimental approaches to the question of AOT–Na^+ hydration permits us on the one hand to confirm some of these data in the literature and on the other hand to gather more insight into the hydration of AOT. The hydration numbers r derived from these three approaches are different varying from 4 to 13 (Table I). This variation is not too surprising considering that the basic principles underlying these three methods are very different. Both DSC and ^2H NMR reveal

(53) Quist, P.-O.; Halle, B. *J. Chem. Soc., Faraday Trans. 1* **1988**, *84*, 1033.
(54) Hertz, H. G. In *Water: A Comprehensive Treatise*; Franks, F., Ed.; Plenum Press: New York, 1973; Vol. 3, Chapter 7.
(55) Glueckauf, E. *Trans. Faraday Soc.* **1955**, *51*, 1235.
(56) Angell, C. A. *Annu. Rev. Phys. Chem.* **1983**, *34*, 593.
(57) Chapman, D.; Williams, R. M.; Ladbrooks, B. D. *Chem. Phys. Lipids* **1967**, *1*, 445.
(58) Carlström, G. Ph.D. Thesis, University of Lund, Lund, 1988.

that water of hydration occurs in different hydration shells and two water molecules are more tightly bound to AOT than the rest of the water of hydration. Six water molecules in the hydration shell of AOT-Na^+ are sufficiently perturbed so that freezing is prevented. In contrast to AOT reversed micelles, in aqueous AOT dispersions forming a smectic phase even these six water molecules freeze when the dispersion is cooled at -40 °C. The difference in the thermal behavior of the two AOT systems is ascribed to supercooling taking place in the submicroscopic droplets of AOT reversed micelles.

Acknowledgment. We acknowledge the technical assistance of J. Stäuble and E. Blöchliger. The NMR measurements were carried out by F. Bangerter, and we are indebted to Dr. P. Skrabal for useful discussions. This work was supported by the ETH.

Registry No. AOT, 577-11-7; isooctane, 540-84-1.

Influence of Multipolar Correlations and Surface Imperfections on the Efficiency of Diffusion-Controlled Reactive Processes on Molecular Organizates and Colloidal Catalysts

Joseph B. Mandeville,† David E. Hurtubise,‡ Richard Flint,‡ and John J. Kozak*

Department of Chemistry, Franklin College of Arts and Sciences, University of Georgia, Athens, Georgia 30602 *(Received: January 20, 1989; In Final Form: May 9, 1989)*

A stochastic-mechanical lattice model is introduced and extensive calculations are performed to assess the role of multipolar correlations and surface imperfections in influencing the efficiency of encounter-controlled reactive processes on the surface of a molecular organizate or colloidal catalyst particle. The change in the diffusion-controlled rate constant k_D in the presence and absence of a down-range biasing potential $v(r)$ [specifically the quantity $k_D(v = v(r))/k_D(v = 0)$] for a reactant pair subject to a short-range chemical (or cage) effect is studied as a function of system size, concentration of defects, medium temperature, and dielectric constant. For $d = 2$ dimensional surfaces of Euler characteristic $\chi = 2$ ("shells") or $\chi = 0$ ("planes"), if the length parameter r characterizing the spatial extent of the system is larger than the (generalized) Onsager length s, the long-range attractive Coulombic potential is, as expected, more effective in enhancing the reaction efficiency than the short-range (angle-averaged) ion-dipole or dipole-dipole potentials. However, both for "shells" and "planes" when the size of the system is decreased or the $d = 2$ reaction space otherwise restricted (so that the lengths r and s are of comparable magnitude), not only can short-range attractive potentials compete in effectiveness with long-range potentials but also, for a given potential, the interplay between these two scale parameters can produce inversions in the reaction efficiency. The role of repulsive potentials in influencing the reaction efficiency is straightforward: the reaction time increases with increase in the strength of the potential with the influence on the reaction rate (much) more pronounced than for attractive potentials. Finally, the relevance of our study to two experimental systems [the dismutation reaction of Br_2^- ion radicals in aqueous solution in the presence of CTAB micelles and the photochemical production of H_2 from water via the reaction of the reduced radical cation of methyl viologen with a colloidal platinum catalyst (Pt_c)] is brought out.

I. Introduction

The surface of a colloidal catalyst particle or molecular organizate (such as micelle, vesicle, or cell) is not smooth and continuous, but rather differentiated by the geometry of the constituents and, if the surface composition is not homogeneous, often organized into domains or clusters. To explore the consequences of such structure on the efficiency of surface-mediated, encounter-controlled reactive processes, we developed recently a lattice-based stochastic model (described below) sufficiently general that the influence of spatial structure on the dynamics could be assessed in detail.[1,2]

We considered a polyhedral surface characterized by dimension $d = 2$ and Euler characteristic $\chi = 2$ [where χ is defined by $\chi = F - E + V$, with F, E, and V the number of faces (cells), edges, and vertices of the polyhedral complex], with N distinct sites on the surface organized into an array defined locally by the site valency ν (or connectivity) of the resulting network. Given this structure we considered a target molecule A anchored to the surface at one of the N sites, a coreactant B free to migrate among the $N - 1$ satellite sites and then analyzed the dynamics of the diffusion-controlled irreversible reaction, $A + B \rightarrow C$. This was done by formulating a stochastic master equation for each geometry considered [in ref 1 and 2 we focused on the polyhedral surfaces defined by the 5 Platonic solids and 16 Archimedean solids] and solved this equation numerically for two classes of initial conditions. Specifically, we determined the survival probability $\rho(t)$ versus time t of the diffusing coreactant B and in addition calculated the first four moments of the probability distribution function describing the process. From the consequent evolution curves, we extracted the individual relaxation times t_0 and from these and the associated moments we were able to identify and quantify the separate influences of the variables N and ν on the kinetics. We found that for fixed N, the time t_0 decreased with increase in the (global or local) valency ν and, secondly, for a given local symmetry (ν fixed), the t_0 increased with N in (almost) all cases.

The purpose of the present study is to broaden this earlier discussion in two ways. The first is to determine the extent to which surface imperfections can influence the efficiency of an encounter-controlled reactive process relative to the situation where the surface is free of defects. Our second objective will be to assess the role of multipolar correlations in modulating the efficiency of surface-mediated reactive processes; in addition to considering short-range forces (viz. chemical or cage effects) we shall also consider the diffusing coreactant B and the target molecule A to

† Department of Physics, University of Illinois, Urbana, IL 61801.
‡ Department of Mathematics, University of Notre Dame, Notre Dame, IN 46556.

(1) Politowicz, P. A.; Kozak, J. J. *Proc. Natl. Acad. Sci. U.S.A.* **1987**, *84*, 8175-8179.
(2) Politowicz, P. A.; Garza-Lopez, R. A.; Hurtubise, D. E.; Kozak, J. J. *J. Phys. Chem.* **1989**, *93*, 3728-3735.

0022-3654/89/2093-7876$01.50/0